Thin-Film Molecular Materials Based on Tetrametallic "Squares": Nanoscale Porosity and Size-Selective Guest Transport Characteristics

Suzanne Bélanger, Joseph T. Hupp,* Charlotte L. Stern, Robert V. Slone, David F. Watson, and Thomas G. Carrell

Contribution from the Department of Chemistry, Northwestern University, Evanston, Illinois 60208

Received August 19, 1998

Abstract: Described are the preparation and functional characterization of nanocrystalline and/or amorphous thin films comprising of neutral "molecular squares" of the form $[Re(CO)_3(Cl)(\mu\text{-L})]_4$ (L = difunctional imine or azine ligand). The films are strongly adherent, stable in aqueous media, and characterized by comparatively few pinhole defects. Electrochemical transport experiments show that the materials are exceptionally porous with respect to sufficiently small solution-phase permeants but blocking toward larger permeants. Related thin-film experiments based on monometallic "corner" materials indicate efficient exclusion of all candidate permeant molecules evaluated. For the title materials, these experiments, together with additional electrochemical probe experiments, indicate that (1) membranelike permeation via pores or tunnels of about nanometer diameter is the primary mode of transport of molecular and ionic species through thin films and (2) the transport-relevant pore or tunnel diameter is defined by the cavity dimensions for the component molecular square. The crystal structure of a single isomer of $[Re(CO)_3(Cl)(\mu\text{-4,4}'\text{-bipyridine})]_4$ is also reported. A packing view down the *c* axis of the tetragonal unit cell shows that the molecules, which are significantly puckered in the crystalline state, are arranged with cavities aligned to generate infinite zeolite-like channels.

Introduction

One of the most exciting recent developments in inorganic host/guest chemistry has been the elaboration of the synthetic chemistry of cavity-containing "molecular square" assemblies. Indeed, several dozen molecular squares and related species based on cis-coordinated metal ion corners and difunctional ligand edges have now been reported.[1−11] The available square assemblies range in size (minimum cavity diameter) from less than 5 Å to greater than 30 Å, with selected assemblies displaying useful ancillary properties such as optical activity[12] or photoluminescence capabilities.[5,13] Perhaps the greatest functional design focus, however, has been on induction of solution-phase recognition and binding properties, where the binding targets range from small planar aromatic species[1,2,14−17] to complex inorganic anions,[5,18] alkali metal cations,[19] and di- and tetrafunctional porphyrin species.[7] The obvious technical drivers are chemical sensing, chemical catalysis, and phase-transfer catalysis.

We reasoned that many of the proposed or demonstrated solution-phase applications could be usefully extended to interfacial or solid-state environments. An interfacial approach clearly would simplify the necessary eventual separation of host species from reaction environments. At the same time, it might open up additional applications for molecular host compounds, such as ultrafiltration, gated transport, or catalytic membrane reactivity.[20,21] We further reasoned that these particular applications might be best explored in a thin-film materials configuration, since rates of transport of molecular species through porous materials typically scale inversely with transport distance

(1) Fujita, M.; Yakazi, J.; Ogura, K. *J. Am. Chem. Soc.* **1990,** *112,* 5645.
(2) Fujita, M.; Yakazi, J.; Ogura, K.; Ogura, K. *Tetrahedron Lett.* **1991,** *32,* 5589.
(3) Fujita, T.; Sasaki, O.; Mitsuhashi, T.; Fujita, T.; Yagazi, J.; Yamaguchi, K.; Ogura, K. *J. Chem. Soc., Chem. Commun.* **1996,** 1535.
(4) Stang, P.; Olenyuk, B. *Acc. Chem. Res.* **1997,** *30,* 502 and references therein.
(5) Slone, R. V.; Yoon, D. I.; Calhoun, R. M.; Hupp, J. T. *J. Am. Chem. Soc.* **1995,** *117,* 11813.
(6) Slone, R. V.; Hupp, J. T.; Stern, C. L.; Albrecht-Schmitt, T. E. *Inorg. Chem.* **1996,** *35,* 4096.
(7) Slone, R. V.; Hupp, J. T. *Inorg. Chem.* **1997,** *36,* 5422.
(8) Leung, W.-H.; Cheng, J. Y. K.; Hun, T. S. M.; Che, C.-M., Wong, W.-T.; Cheung, K. K., *Organometallics* **1996,** *15,* 1497.
(9) Kalb, W. C.; Demidowicz, Z.; Speckmann, D. M.; Knobler, C.; Teller, R. G.; Hawthorne, M. F. *Inorg. Chem.* **1982,** *21,* 4027.
(10) Stricken, P. M.; Volcko, E. J.; Verkade, J. G. *Inorg. Chem.* **1983,** *105,* 2494.
(11) Rauter, H.; Hillgeris, E. C.; Erxleben, A.; Lippert, B. *J. Am. Chem. Soc.* **1994,** *116,* 616.
(12) Olenyuk, B.; Whiteford, J. A.; Stang, P. J. *J. Am. Chem. Soc.* **1996,** *118,* 8221.
(13) Slone, R. V.; Benkstein, K. D.; Bélanger, S.; Hupp, J. T.; Guzei, I. A.; Rheingold, A. L. *Coord. Chem. Rev.* **1998,** *171* (1), 221.

(14) Fujita, M.; Nagao, S.; Iida, M.; Ogata, K. *J. Am. Chem. Soc.* **1993,** *115,* 1574.
(15) Stang, P. J.; Cao, D. H.; Saito, S.; Arif, A. M. *J. Am. Chem. Soc.* **1995,** *117,* 6273.
(16) Stang, P. J.; Cao, D. H. *J. Am. Chem. Soc.* **1994,** *116,* 4981.
(17) Fujita, M.; Nagao, S.; Ogura, K. *J. Am. Chem. Soc.* **1995,** *117,* 1649.
(18) See also: Beer, P. D. *J. Chem. Soc., Chem. Commun.* **1996,** 689.
(19) Stang, P. J.; Cao, D. H.; Chen, K.; Gray, G. M.; Muddiman, D. C.; Smith, R. D. *J. Am. Chem. Soc.* **1997,** *119,* 5163.
(20) For elegant illustrations of such applications with mesoporous membranes of a different type (metal and carbon nanotubules), see: (a) Nishizawa, M.; Menon, V. P.; Martin, C. R. *Science* **1995,** *268,* 700. (b) Jirage, K. B.; Hulteen, J. C.; Martin, C. R. *Science* **1997,** *278,* 655. (c) Che, G.; Fisher, E. R.; Martin, C. R. *Nature* **1998,** *393,* 346.
(21) For representative reports on gated charge transport through polymeric thin films and electrode-supported monolayers, respectively, see: (a) Burgmayer, P.; Murray, R. W. *J. Am. Chem. Soc.* **1982,** *104,* 6139. Burgmayer, P.; Murray, R. W. *J. Electroanal. Chem.* **1983,** *147,* 339. Burgmayer, P.; Murray, R. W. *J. Phys. Chem.* **1984,** *88,* 2515. (b) Campbell, D.; Herr, B. R.; Hulteen, J. C.; VanDuyne, R. P.; Mirkin, C. A. *J. Am. Chem. Soc.* **1996,** *118,* 10211.

Chart 1
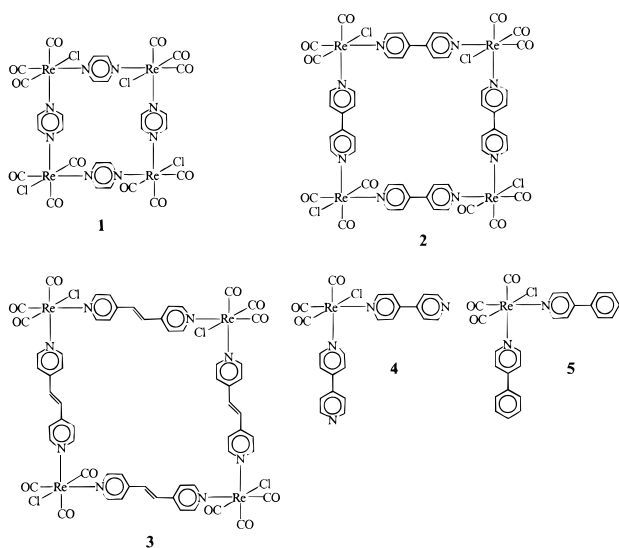
(material thickness).[22] Here we report on the preparation and functional characterization of thin-film versions of molecular materials comprising of selected tetrarhenium square assemblies, as well as related corner assemblies (cf. compounds **1**−**5**, Chart 1). We also report on the single-crystal structure of one of the molecular materials. These particular materials were chosen, in part, because prior X-ray structural studies had already pointed toward a propensity for extended, one-dimensional channel formation.[6] The materials were also attractive because of the charge neutrality of the various molecular components and the resulting absence of channel-blocking counterions.[13,15,23,24] Finally, the tendency for the compounds to dissolve in polar organic solvents—while completely resisting dissolution in water —suggested comparatively simple thin-film processing protocols and subsequent condensed-phase characterization protocols.

As shown below, we find that transport through the available thin films can be readily monitored and at least partially quantified by utilizing aqueous electrochemical measurement techniques. Briefly, we have made use of soluble, redox-active, permeant species of varying size and charge. By then preparing candidate films on electronically conductive platforms (e.g., gold or glassy carbon electrodes), we have taken advantage of the requirement that a particular probe molecule fully traverse the film material in order to undergo electrochemical oxidation or reduction.[25] The electrochemical process, of course, is then observable as a potential-dependent flow of current. The electrochemical measurements show that thin films based on neutral tetrametallic squares are capable of functioning as comparatively efficient molecular sieves. (For example, diffusion through the "squares" membranes is substantially faster (more efficient) than diffusion through chemically related metallopolymeric membranes.) Furthermore, the sieving phenomenon is

characterized by sharp molecular size cutoffs,[26] where the cutoffs are (1) predictable based on the X-ray or model determined cavity diameters for the component square compounds and (2) adjustable on the basis of straightforward synthetic variations. We note that the molecular sieving properties of the molecular squares films are not exclusive to these materials: some organic polymers,[27−30] as well as metallopolymers,[31−35] display molecular sieving toward variable-size permeants. However, for the polymer systems, which are typically cationic, the molecular size cutoff is not easily predictable (i.e., fine-tuning of the permeation cutoff is difficult), since it depends, among other things, on the extent of cross-linking[36] and on the nature of the counterions incorporated in the film during the polymerization.[37,38] Sharp molecular-size cutoffs have also been reported for free-standing nanotube-based molecular filtration membranes,[20b] as well as porous lipid bilayers containing peptide nanotubules.[39−41] The nanotubule membranes, like the thin films based on the molecular squares, are potentially more attractive than the polymer systems in the sense that they readily allow for monodisperse pore sizes and predictable molecular-size cutoffs. We suggest that the size-selective transport properties reported here may prove useful in subsequent catalytic applications, ultrafiltration applications, and chemical sensing applications.[20,21]

Experimental Section

Materials. Neutral, tetrarhenium-based squares featuring pyrazine (pz, **1**), 4,4′-bipyridine (4,4′-bpy, **2**), or *trans*-1,2-bis(4-pyridyl)ethylene (bpe, **3**) and mononuclear Re(CO)$_3$(Cl)(L)$_2$ complexes, where L is 4,4′-bipyridine (**4**) or 4-phenylpyridine (**5**), were prepared via literature methods.[6,42] Aqueous solutions of [Fe(LL)$_3$]SO$_4$ (LL = 2,2′-bpy (2,2′-bipyridine), phen (1,10-phenanthroline), and bphenSO$_3$Na (bathophenanthrolinedisulfonic acid, sodium salt)) were purchased from GFS Chemicals. (The bphenSO$_3$Na ligand is manufactured as a mixture of isomers with respect to the position of the sulfonate group on the phenyl subtituent. The resulting Fe(bphenSO$_3$)$_3^{4-}$ complex is, therefore, also

(22) Baker, R. W.; Cussler, E. L.; Eykamp, W.; Koros, W. J.; Riley, R. T.; Strathmann, H. *Membrane Separations Systems, Recent Developments and Future Directions*; Noyes Data Corp.: Park Ridge, IL, 1991.

(23) Stang, P. J.; Chen, K.; Arif, A. M. *J. Am. Chem. Soc.* **1995**, *117*, 8783.

(24) Whiteford, J. A.; Lu, C. V.; Stang, P. J. *J. Am. Chem. Soc.* **1997**, *119*, 2524.

(25) The requirement can be circumvented, of course, if defects (holes) exist, if permeant redox self-exchange reactions are significant, or if the film itself becomes electronically conductive.

(26) Here, and elsewhere in the report, "sharp molecular cutoffs" is meant to indicate abrupt, as opposed to gradual, permeant size discrimination. The description is *not* meant to imply that perfect molecular sieving (i.e., leak-free sieving) is achieved. Indeed, as indicated below, some leakage, apparently defect-based, is observed with each of the five molecular materials described here. In contrast, zero leakage has been detected in ultrafiltration experiments invoking membranes based on metal-plated nanotubules.[20b]

(27) Ohnuki, Y.; Matsuda, H.; Ohsaka, T.; Oyama, N. *J. Electroanal. Chem.* **1983**, *158*, 55.

(28) Ohsaka, T.; Hirokawa, T.; Miyamoto, H.; Oyama, N. *Anal. Chem.* **1987**, *59*, 1758.

(29) Taj, S.; Ahmed, M F.; Sankarapapavinasam, S. *Ind. J. Chem.* **1993**, *32A*, 521.

(30) McCarley, R. L.; Irene, E. A.; Murray, R. W. *J. Phys. Chem.* **1991**, *95*, 2492.

(31) Ikeda, T.; Schmehl, R.; Denisevidch, P.; Willman, K.; Murray, R. W. *J. Am. Chem. Soc.* **1982**, *104*, 2683.

(32) Gough, S.; Strouse, G. F.; Meyer, T. J.; Sullivan, B. P. *Inorg. Chem.* **1991**, *30*, 2942.

(33) Gould, S.; Meyer, T. J. *J. Am. Chem. Soc.* **1991**, *113*, 7442.

(34) Pressprich, K. A.; Maybury, S. G.; Thomas, R. E.; Linton, R. W.; Irene, E. A.; Murray, R. W. *J. Phys. Chem.* **1989**, *93*, 5568.

(35) Bélanger, S.; Stevenson, K. J.; Mudhaka, S. A.; Hupp, J. T. *Langmuir*, submitted.

(36) Yan, S. G.; Hupp, J. T. *J. Electroanal. Chem.* **1995**, *397*, 119.

(37) Cosnier, S.; Deronzier, A.; Roland, J.-F. *J. Electroanal. Chem.* **1991**, *310*, 71.

(38) Lyon, L. A.; Ratner, M. A., Hupp, J. T. *J. Electroanal. Chem.* **1995**, *387*, 109.

(39) Ghadiri, M. R.; Granja, J. R.; Buehler, L. K. *Nature* **1994**, *369*, 301.

(40) Granja, J. R.; Ghadiri, M. R. *J. Am. Chem. Soc.* **1994**, *116*, 10785.

(41) Hartgerink, J. D.; Clark, T. D.; Ghadiri, M. R. *Chem. Eur. J.* **1998**, *4*, 1367.

(42) Giordano, P. J.; Wrighton, M. S. *J. Am. Chem. Soc.* **1979**, *101*, 2888.

a mixture of isomers; it was used without purification.) [Co(2,2'-bpy)$_3$]-(NO$_3$)$_2$ and [Co(phen)$_3$](NO$_3$)$_2$ were prepared from Co(NO$_3$)$_2$·6H$_2$O in ethanol as described in the literature for the perchlorate analogues.[43] [Ru(NH$_3$)$_5$(4-pic)](PF$_6$)$_2$ (4-pic = 4-picoline) and [Ru(NH$_3$)$_5$(py)]Cl$_2$ (py = pyridine) were prepared according to literature methods.[44] (For chemical structures of permeants, see Chart 1, below.) Solvents (reagent grade) were from Fischer. All other chemicals were from Mallinckrodt or Aldrich.

Film Preparation. In a typical film preparation, a saturated solution of the molecular square is prepared in acetonitrile (**1**) or acetone (**2**, **3**). The suspension is sonicated, and an equal volume of chloroform is added. The suspension is filtered on a 0.1-μm poly(tetrafluoroethylene) membrane (Whatman), and a few drops of the resulting solution are placed on the electrode and left to evaporate slowly, with slow rotation (100−200 rpm) of the electrode. Films of the Re(CO)$_3$(Cl)(L)$_2$ monomers are prepared by the same technique, but from 1:1 (v/v) acetone/CHCl$_3$ solutions. Since the monomers (corners) are much more soluble than the squares, filtration is unnecessary. Solutions of the 4,4'-bpy corners in acetone/CHCl$_3$ should be used within a few hours, as the monomer (in the presence of a weakly coordinating solvent) has been found to transform eventually into the corresponding square.[13] Permeation studies were effected after a film drying time of 20−30 min (necessary to ensure good adhesion to the electrode surface). The films retain sieving properties for at least several hours in aqueous medium. Repetitive scanning of permeant solutions, however, some-times led to film degradation. Therefore, a new film was prepared for each permeation experiment.

Film Thickness Determination. The thickness of the films was determined to be in the 0.15−2.5-μm range. Thickness was estimated by (1) dissolving the film material in a known volume of acetonitrile following the electrochemical experiment, (2) recording an electronic absorption spectrum, (3) using the absorbance value at the following metal-to-ligand charge-transfer band[13] extinctions (M^{-1} cm^{-1}), 1.9 × 10^4 (**2**), 2.3 × 10^4 (**3**), and 4.5 × 10^4 (**4**), to determine the amount of material present, and 4) assuming the most dense packing possible for the films, i.e., the following dimensions for the squares (Å): 19 × 19 × 7 (**2**), 21 × 21 × 7 (**3**), and (12 × 12 × 7)/2 (**4**). Note that this assumption does not take into account that molecule **4** can, in principle, interpenetrate. If so, film thicknesses for this material may be overestimated.

Electrochemical Measurements. An EG&G PAR 273 or 264 potentiostat and a Houston Instruments $x-y$ recorder (model 2000) were used for electrochemical measurements. A 3-mm glassy carbon (GC) electrode (Cypress) or a 3-mm GC or gold rotating disk electrode tip (Bioanalytical Systems), adapted to fit a Pine Instruments analytical rotator (model MSRX), was used for permeation studies. Distilled and purified (Millipore) water was used to prepare the permeant solutions; these were typically 5−10 mM in electroactive species and 0.5−1 M in KNO$_3$. Electrochemical measurements were conducted with a conventional one-compartment, three-electrode setup (platinum wire counter electrode, saturated sodium chloride calomel reference electrode (SSCE)). The scan rate of the rotating disk electrode (RDE) voltam-metry scan was 10 mV/s.

Crystal Structure. Single-isomer crystals of **2**·0.5(CH$_3$)$_2$CO (see below) were obtained from slow evaporation of an acetone solution. Reflections were collected on an Enraf-Nonius CAD-4 diffractometer using graphite-monochromated Mo Kα radiation. The *I*-centered tetragonal cell was refined using 25 reflections (18 < 2θ < 24°). Reflection data were collected up to 2θ = 50° (3385 measured reflections, 3266 unique, 2164 with $I/\sigma(I) > 3$ used for refinement). No decay correction was applied, but intensity data were corrected for absorption (analytical correction,[45] μ = 71.2 cm^{-1}, T_{min} = 0.38, T_{max} = 0.50), Lorentz and polarization effects. A correction for secondary extinction was also applied. The space group (*I*$\bar{4}$) was deduced from the systematic absences (*hkl*, $h + k + l$ ... 2n), statistical analysis of

Table 1. Crystal Data for **2**·0.5(CH$_3$)$_2$CO

chemical formula	C$_{53.5}$H$_{35}$N$_8$Cl$_4$O$_{12.5}$Re$_4$
formula weight	1951.58
crystal system	tetragonal
space group	*I*$\bar{4}$
color	yellow
crystal size, mm	0.15 × 0.14 × 0.13
a, Å	22.72(2)
c, Å	13.538(5)
V, Å^3	6986(6)
Z	4
R, $I > 3\sigma(I)^a$	0.059
wR, $I > 3\sigma(I)^b$	0.060
GOF, $I > 3\sigma(I)$	2.06

^{a} $R = \sum||F_o| - |F_c||/\sum|F_o|$. ^{b} $wR = [(\sum w(|F_o| - |F_c|)^2/\sum wF_o^2]^{1/2}$.

Table 2. Selected Bond Lengths (Å) and Angles (deg) for **2**·0.5(CH$_3$)$_2$CO

Re1−Cl1	2.49(1)	Re2−Cl2	2.48(1)
Re1−N1	2.22(3)	Re2−N3	2.26(3)
Re1−N2	2.22(3)	Re2−N4	2.20(3)
Re1−C11	1.91(3)	Re2−C24	1.9(1)
Re1−C13	1.9(1)	Re2−C26	1.92(4)
Re1−C12	1.99(4)	Re2−C25	1.92(4)
C11−O1	1.14(4)	C24−O4	1.2(1)
C12−O2	1.14(4)	C25−O5	1.18(4)
C13−O3	1.0(1)	C26−O6	1.10(4)
N1−Re1−N2	85(1)	N3−Re2−N4	83(1)
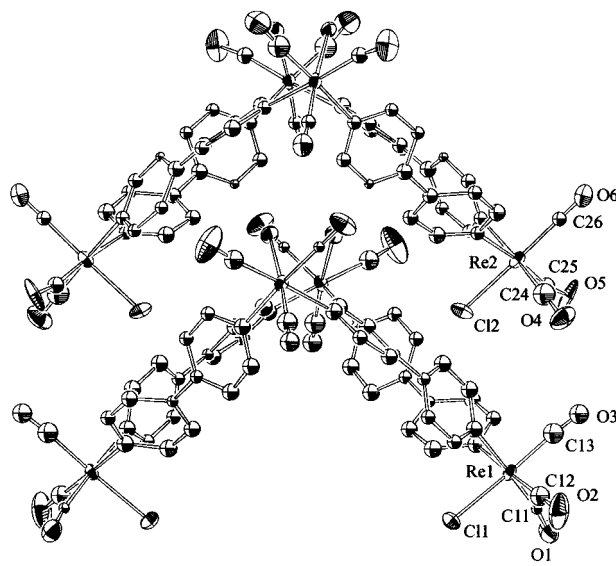
Figure 1. Side view of the two independent square molecules, showing their puckered arrangement. Top view and full numbering scheme available in the Supporting Information.

the distribution of the intensity data, and successful refinement of the structure. The structure was solved by direct methods (SHELXS86[46]). Non-hydrogen atoms were located from successive difference Fourier maps, and hydrogen atoms were calculated at idealized positions, using a riding model. Re, Cl, and O atoms were refined anisotropically. C atoms were refined with isotropic thermal parameters. Atomic scattering factors were taken from the usual sources.[47] Final refinement was done by full-matrix least-squares on F^2 using teXsan.[48]

(43) Wheeler, S. H.; Zingheim, S. C.; Nathan, L. C. *J. Inorg. Nucl. Chem.* **1978**, *40*, 779.

(44) Curtis, J. C.; Sullivan, B. P.; Meyer, T. J. *Inorg. Chem.* **1983**, *22*, 224.

(45) de Meulenaer, J.; Tompa, H. *Acta Crystallogr.* **1965**, *19*, 1014.

(46) Sheldrick, G. M. In *Crystallographic Computing 3*; Sheldrick G. M., Kruger, C., Goddard, R., Eds.; Oxford University Press: New York, 1985; p 175.

(47) *International Tables for Crystallography*; Kynoch Press: Witton, Birmingham, U.K., 1992; Vol. C, Tables 4.2.6.8 and 6.1.1.1.

(48) *teXsan. Single-Crystal Structure Analysis Software*. Version 1.7.MSC, Molecular Structure Corp. 3200 Research Forest Drive, The Woodlands, TX, 1995.
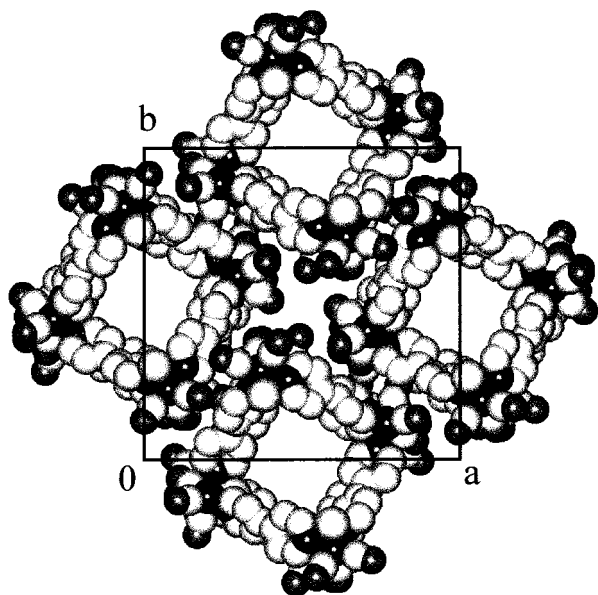
Figure 2. Packing diagram for the single-isomer polymorph of **2** in the *ab* plane, showing the infinite channels along the crystallographic *c* axis. Crystallization solvent (acetone) omitted for clarity.
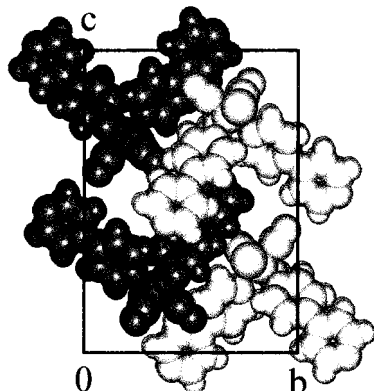

Figure 3. Packing diagram for **4**, in the *bc* plane, showing the absence of channels (from ref 49, arbitrary color scheme).

Results and Discussion

Crystal Structure of Square 2. Synthesis of this species and similar squares yields, in principle, a mixture of isomers with respect to the orientation of the chloride ligands relative to the plane of the four Re atoms. Crystal structures for $[Re(CO)_3$-$(Cl)pz]_4$ (**1**) and $[Re(CO)_3(Cl)4,4'-bpy]_4$ (**2**) have been reported in an earlier communication.[6] In both cases, the structure revealed that the square was planar. The structures further showed Cl/CO disorder in the direction perpendicular to the plane of each molecular square. Whether this reflected cystallization of mixtures of isomers or, instead, disorder caused by crystal packing could not be determined. In this report, the crystal structure of a single isomer of the bipyridine square is described, in which the chloride ligands adopt alternating *up−down* orientations.

Crystal data are collected in Table 1; bond lengths and angles associated with the Re center can be found in Table 2. The unit cell contains two molecules per asymmetric unit. The N−Re−N angles (82(1) and 84(1)°) are similar to those usually observed in molecular squares.[6,13,15] Unlike the molecules comprising the disordered polymorph reported earlier,[6] however, those in the single-isomer crystal are significantly puckered: In molecule 1 of Figure 1, the rhenium atoms are displaced 3.0829(11) Å above and below the average plane of the metal centers. For
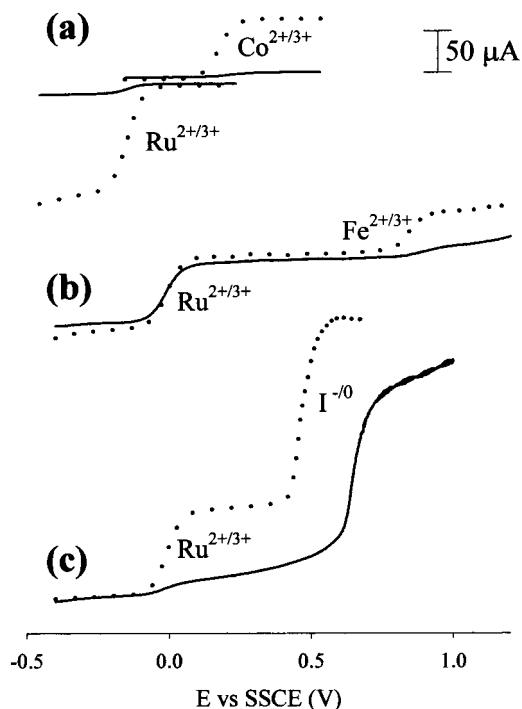
Figure 4. (a) Rotating disk electrode voltammetry of solutions of $Ru(NH_3)_6{}^{3+}$ (5.0 mM) and $Co(phen)_3{}^{2+}$ (5.0 mM) on a bare electrode (•••), and on an electrode coated with a thin film of **4** (−). (b) Analogous experiment performed with a mixture of $Ru(NH_3)_5(4-pic)^{2+}$ (5.2 mM) and $Fe(bphenSO_3)_3{}^{4−}$ (5.0 mM) with a thin film of **3** and at a bare electrode. (c) Analogous experiment performed with a mixture of $Ru(NH_3)_5(4-pic)^{2+}$ (5.9 mM) and $I^−$ (4.5 mM) on a bare electrode and on an electrode coated with a film of **1**. Diameters of permeants: $Fe(bphenSO_3)_3{}^{4−}$, 24 Å; $Ru(NH_3)_5(4-pic)^{2+}$, 6.7 Å; $Ru(NH_3)_6{}^{3+}$, 5.5 Å; $I^−$, 2.4 Å. Re•••Re distance in the molecular squares: **3**, 14 Å; **1**, 7 Å. Scan rate is 10 mV/s; rotation rate of the RDE is 500 rpm, in 1 M KNO_3.
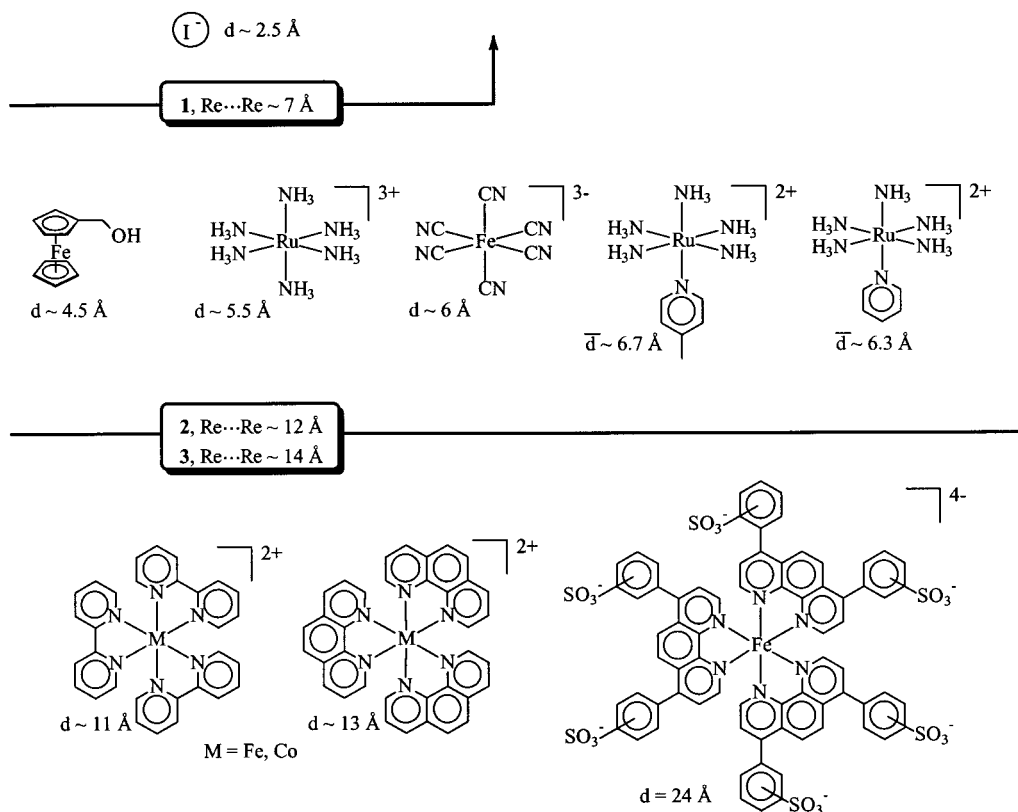
Chart 2
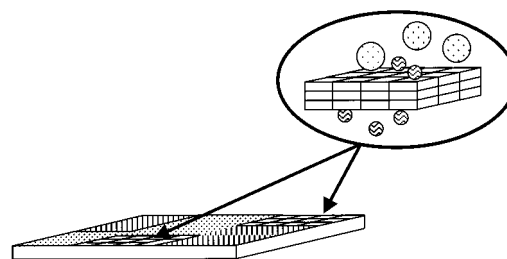
the crystallographically distinct second molecule in Figure 1, the rhenium atoms are displaced by ±3.8614(11) Å. The dihedral angles between the least-squares planes of the pyridine rings are 36.7 and 38.5°. Typical dihedral angles for metallocyclophanes with bridging 4,4′-bpy ligands are in the 25−30° range.[3,6,15] Note that this tilting of the pyridine rings with respect to the walls of the square cavity (as well as the puckering) reduces its effective size. The molecular packing diagram showing the infinite open-end channels along the *c* axis, is represented in Figure 2. Crystallization solvent (acetone) molecules are located along the channels, above and below the molecular squares. Shown for comparison in Figure 3 is a space-filled representation of the packing structure of a single crystal of **4**.[49] Note the absence of channels. The packing structure for **5** similarly lacks channels.[50]

(49) Bélanger, S.; Hupp, J. T.; Stern, C. L. *Acta Crystallogr.* **1998**, *C54*, 1596.

(50) Keefe, M. H. unpublished results.

Chart 3

I^- $d \sim 2.5$ Å

1, Re···Re $\sim$ 7 Å

OH $d \sim 4.5$ Å

$[Ru(NH_3)_6]^{3+}$ $d \sim 5.5$ Å

$[Fe(CN)_6]^{3-}$ $d \sim 6$ Å

$[Ru(NH_3)_5(py)]^{2+}$ $\overline{d} \sim 6.7$ Å

$[Ru(NH_3)_5(py)]^{2+}$ $\overline{d} \sim 6.3$ Å

2, Re···Re $\sim$ 12 Å
3, Re···Re $\sim$ 14 Å

$M(2,2'\text{-bpy})_3^{2+}$ $d \sim 11$ Å   M = Fe, Co

$M(phen)_3^{2+}$ $d \sim 13$ Å

$Fe(bphenSO_3)_3^{4-}$ $d = 24$ Å

Size Selectivity in Thin Films of Molecular Squares. The permeability of the mesoporous materials with respect to approximately a dozen redox-active probe molecules was examined via rotating disk electrode and cyclic voltammetry. Briefly, a thin film of the desired square or corner was cast on the surface of an electrode (see Experimental Section), and the potential-dependent current for oxidation or reduction of an aqueous solution of the probe molecule was monitored under hydrodynamically well-defined conditions.[51] In principle, electroactive species could reach the electrode by diffusion through defects in the film (pinholes or cracks). Since the dimensions of such defects are presumably larger than those of the candidate molecular permeants, transport through them is expected to be independent of the size of the permeant, and size selectivity should not be observed. Alternatively, they can reach the electrode by permeation, i.e., solution-to-film partitioning, followed by diffusion through film pathways of molecular dimensions whose size are limited to that of the molecular square. In any case, one way to distinguish between pathways of molecular dimensions and diffusion via pinholes or cracks is to show size exclusion. As suggested by Chart 2, the relevant dimensions could be those of the aligned molecular squares. As also suggested by the chart, there may well exist regions of the film where transport is inhibited (by channel blockage or disorder) or unproductive (channels oriented parallel rather than perpendicular to the film).

Size exclusion is shown experimentally in Figure 4. Figure 4b shows comparisons of the RDE signal observed for an aqueous mixture of $Ru(NH_3)_5(4\text{-pic})^{2+}$ and $Fe(bphenSO_3)_3^{4-}$ at a GC electrode coated with a thin film of **3** (Re···Re ca. 14 Å),

and a bare electrode. The experiment clearly shows that the smaller ruthenium complex ($d \sim 6.7$ Å) passes readily through the film comprising of the molecular square **3**, while the larger iron complex ($d \sim 24$ Å) is excluded.[52] The relative magnitude of the residual signal observed for the iron permeant varied from film to film and is attributed, therefore, to transport through pinhole defects. Figure 4a shows a similar experiment with a thin film of **4**, in contact with solutions of $Ru(NH_3)_6^{3+}$ and $Co(phen)_3^{2+}$. Note that, in the case of the corner molecule **4**, the magnitude of the current is greatly decreased by the presence of the film, for both the small Ru and the large Co permeants, and that the relative intensity of the current for both species is the same, regardless of film thickness. These results indicate that films of **4** are almost completely blocking toward these permeants and that they do not exhibit size selectivity. Figure 4c shows an analogous experiment with a thin film of **1** (Re···Re $\sim$7 Å), with $Ru(NH_3)_5(4\text{-pic})^{2+}$ and I^- as permeants: only the smaller permeant ($d \sim 2.4$ Å) is transported through the film. Other experiments indicate that films of **2** and **3** are permeable to ferrocenemethanol ($d \sim 4.5$ Å), $Ru(NH_3)_6^{3+}$ ($d \sim 5.5$ Å), ferricyanide ($d \sim 6$ Å), $Ru(NH_3)_5(py)^{2+}$ ($d_{av} \sim 6.3$ Å), and $Ru(NH_3)_5(4\text{-pic})^{2+}$ ($d_{av} \sim 6.7$ Å), but not to $M(2,2'\text{-bpy})_3^{2+}$ or $M(phen)_3^{2+}$ (M = Fe, Co; $d \sim 11$ and 13 Å, respectively). These size cutoffs, illustrated in Chart 3, are consistent with the internal dimensions of the squares.[53] The experiments strongly suggest, therefore, that permeation is governed by transport through individual square cavities rather than through *inter*molecular interstices. The experiments also imply that channels exist—or, at least, that herringbone packing or other blockage of square

(51) The one-electron oxidation of Re(I) is observed in solution at potentials higher that 1.3 V vs SSCE, and a one-electron ligand-based reduction is present below −0.9 V vs SSCE (see ref 13). The molecular squares are electrochemically silent in the potential range investigated here, and no interfering signal from the squares is observed.

(52) Since the molecular squares are neutral, permeation should not be affected by the charge of the permeant. We nevertheless verified that the large $Fe(bphenSO_3)_3^{4-}$ complex is size-excluded, rather than excluded on the basis of its large negative charge, by showing that the small, but highly charged ferricyanide anion does in fact permeate under analogous conditions.

cavities does not dominate the film configuration.[54] Despite the available structures, these findings were not a foregone conclusion: Unpublished atomic force microscopy and polarized absorption microscopy studies indicate that cast films are typically either largely amorphous or nanocrystalline (~300 nm crystallite size) rather than micro-crystalline. (The precise structural form appears to depend strongly on the choice of solvent for casting and evaporation.[55]) We further observe that the blocking behavior encountered for amorphous or polycrystalline thin films of "corner" compounds, **4** and **5**, was also not a foregone conclusion, despite the available single-crystal structures.

Membrane Diffusion. To obtain quantitative descriptions of the permeability of metallocyclophane-derived molecules, we invoked a membrane diffusion model. The model views the overall transport process simply as consecutive solution-phase mass transport and membrane permeation processes. If transport is monitored electrochemically at a rotating disk electrode, the observed limiting current can be written as the reciprocal sum of the currents (or rates) for the component solution and film-based processes:[31,56–59]

$$i_{lim}^{-1} = i_{mass\ transport}^{-1} + i_{permeation}^{-1} \qquad (1)$$

where

$$i_{mass\ transport} = 0.620nFAD^{2/3}\omega^{1/2}\nu^{-1/6}C_{soln} \qquad (2)$$

$$i_{permeation} = nFAPD_{film}C_{soln}/d \qquad (3)$$

In the equations, n is the number of electrons transferred per permeant, F is the Faraday constant, A is the electrode area, D is the diffusion coefficient of the permeant in solution, ω is the rotation rate of the electrode, ν is the kinematic viscosity of the solvent, C_{soln} is the solute concentration, and d is the film thickness. The permeability of the film is characterized by PD_{film}, where P is the partition coefficient of the solute ($P = C_{film}/C_{soln}$, where C_{film} is the solute concentration in the film), and D_{film} is its diffusion coefficient within the film. This model assumes uniform diffusion (via pathways of molecular dimensions) in all regions of a porous film (however, see Chart 2), as opposed to transport through defects (pinholes or cracks) much larger than molecular dimensions in an otherwise nonporous membrane.

From eqs 2 and 3, the component currents can be separated by systematically varying the electrode rotation rate and,

(53) Note that the effective size of the cavity is smaller than the Re···Re distance, because of the tilt of the bridging rings relative to the square cavity walls and because of finite van der Waals radii. Note that the effective diffusion coefficients of nonspherical molecules in solution are proportional to their average diameters (see: Koval, C. A.; Ketterer, M. E.; Reidsema, C. M. *J. Phys. Chem.* **1986**, *90*, 4201.) In thin-film materials, the permeant molecule could, in principle, rotate faster than it diffuses (i.e., the film could exhibit shape selectivity if the molecule can tumble fast enough for the permeation to be dominated by the smallest molecular dimension).

(54) Although we cannot absolutely exclude the alternative intermolecular permeation pathway, it is unlikely that the size cutoff for permeation between molecular squares would vary with the molecular squares' dimensions. Furthermore, quantitative data on the corner molecule **4** (where permeation is expected to take place mainly through such intermolecular pathways) show that permeation via this mechanism is at least 1 order of magnitude lower than for the parent square **2**.
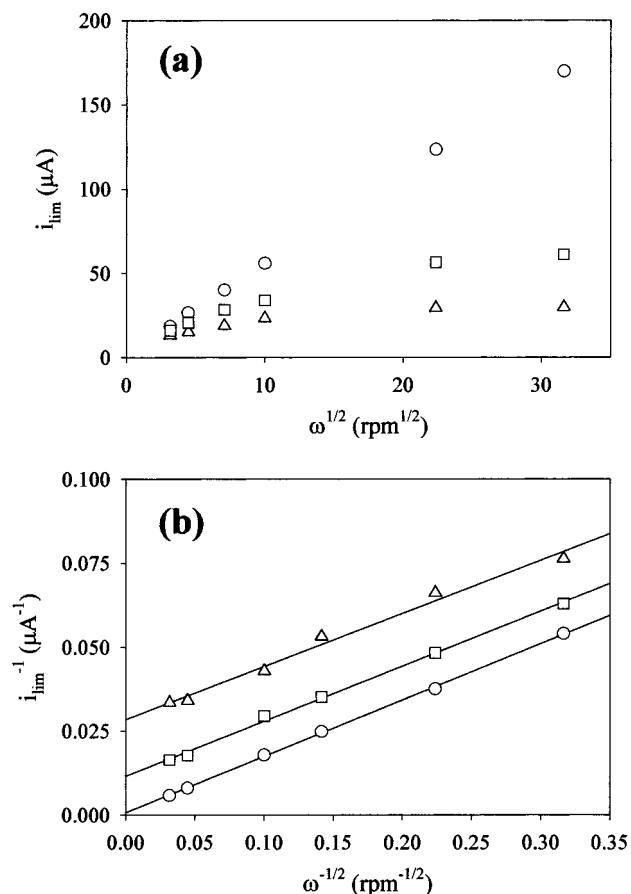
(55) Stevenson, K. J.; Bélanger, S., unpublished studies.

(56) Gough, D. A.; Leypoldt, J. K. *Anal. Chem.* **1979**, *51*, 439.

(57) Leddy, J. A.; Bard, A. J. J. *Electroanal. Chem. Interfacial Electrochem.* **1983**, *153*, 223.

(58) Ewing, A. G.; Feldman, B. J.; Murray, R. W. *J. Phys. Chem.* **1985**, *89*, 1263.

(59) Savéant, J.-M. *J. Electroanal. Chem.* **1991**, *302*, 91.

Figure 5. Levich (a) and Koutecky−Levich (b) plots for 7.2 mM Ru-(NH$_3$)$_5$py^{2+} on a bare electrode (○) and on electrodes covered with thin films of **2** ($d = 0.1$ μm (□); $d = 0.7$ μm (△)).

therefore, the rate (or current) for solution-phase mass transport (forced convection). Figure 5a illustrates the limiting voltammetric responses from a Ru(NH$_3$)$_5$py^{2+} solution at a naked GC electrode, an electrode coated with a comparatively thin film of **2**, and an electrode coated with a thicker film of **2**, each as a function of $\omega^{1/2}$. Note that for the naked electrode the plot is linear, as expected if only solution-phase mass transport is involved. The curved plots for the film-covered electrodes indicate mixed control, with forced convection limiting the transport at low rotation rates and film permeation limiting the transport at high rotation rates. The difference in limiting currents in the rotation rate-insensitive portion of the plots indicates that the thicker film poses a more substantial permeation barrier.

If the film thickness is known, the permeability (PD_{film}) can be determined from the current obtained at limiting high rotation rates or more reliably from the slope of a plot of i_{perm} vs $1/d$ (eq 3). Needed permeation currents were obtained from the intercepts of plots of $i_{lim} - 1$ vs $\omega^{-1/2}$ (Koutecky−Levich plots; Figure 5b). Figure 6 shows a plot of permeation current vs inverse film thickness for transport of Ru(NH$_3$)$_5$py^{2+} through films of **2**. Also illustrated is the blocking behavior toward the candidate permeant Ru(NH$_3$)$_6$$^{3+}$ by films comprising of the low-porosity "corner" compound **4**.[60] Returning to the porous films

(60) The experiment with **4** was carried out in pH 8 buffer to ensure that the free pyridine site on the 4,4′-bpy ligand remained unprotonated. Protonation of this site would lead to a cationic film, which could exclude the Ru permeant-based ion charge (not size). Additional experiments (not shown) on the 4-phenylpyridine analogue **5**, where the free pyridine ring of the 4,4′-bpy ligand is replaced by a (pH-independent) phenyl ring, revealed similar transport blocking behavior.
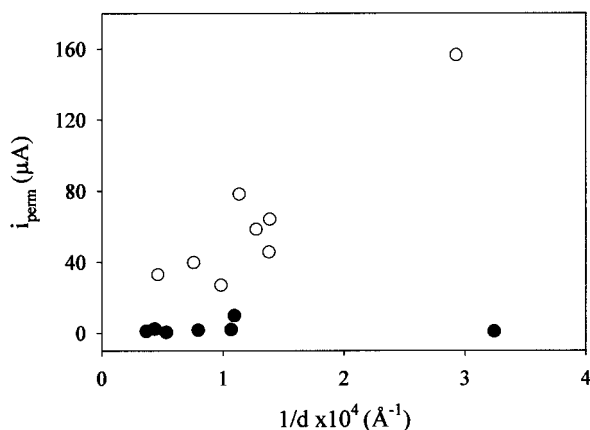
Figure 6. Comparison of the permeation rates (currents) for thin films of corners and of molecular squares as a function of inverse film thickness: $Ru(NH_3)_5py^{2+}$ with square **2** (○) and $Ru(NH_3)_6^{3+}$ with corner **4** (●).

composed of **2**, the plot in Figure 6 yields a PD_{film} value of 3 $\pm$ 1 $\times$ 10^{-7} cm^2 s^{-1}.[61] The significant scatter in the plot probably reflects residual contributions from pinhole transport, which can vary from film to film.[62] Similar plots for $Fe(CN)_6^{3-}$ (not shown) yielded a PD_{film} value of $(0.9 \pm 0.3) \times 10^{-7}$ cm^2 s^{-1} for permeation of films composed of **2** and $(0.8 \pm 0.5) \times 10^{-7}$ cm^2 s^{-1} for films composed of the slightly larger square **3**. While the RDE experiments provide no information about P and D_{film} separately, it seems reasonable to assume for the hydrophilic permeant complexes examined here that the solution/ film partition coefficients are not particularly large.

A comparison of the measured permeabilities for $Fe(CN)_6^{3-}$ and $Ru(NH_3)_5py^{2+}$ to the corresponding solution-phase diffusion coefficients shows that the former are $1-2$ orders of magnitude smaller.[63] On the other hand, the permeabilities are $\sim$1 order of magnitude *larger* than typically observed with amorphous metallopolymeric films featuring pores of similar size (for example, poly[Ru(4-vinyl-4′-methyl-2,2′-bipyridine)$_3^{2+}$][31] and poly[Fe(5-amino-1-10-phenanthroline)$_3^{2+}$][35,36]). The difference presumably reflects both the differences in short range order

for the polymeric vs molecular materials and the presence of charge-compensating anions within the metallopolymeric materials.[64]

Conclusion

The single isomer crystal structure of square **2** shows a puckered arrangement, with infinite zeolite-like channels. The corresponding nanocrystalline and/or amorphous thin-film materials, obtained by slow evaporation of solutions of **2** or other squares, show high mesoporosity and relatively low incidences of defects. The films are strongly adherent, stable in aqueous media, and generally retain their porosity even after several hours in water. Size cutoff data from electrochemical probe experiments indicate that membranelike permeation via pores or tunnels of molecular dimensions is the primary mode of transport of molecular and ionic species through the films. The probe experiments also show that the transport-relevant pore or tunnel size is defined by the cavity dimensions for the component molecular square. The eventual preparation of squares where the bridging ligand is tailored to have a high affinity for a particular type of permeant (i.e., discrimination based on chemical interactions), or the eventual preparation of molecular rectangles (discrimination based on shape), could make these materials genuinely attractive for molecular recognition and separations applications.

Supporting Information Available: ORTEP views of the two crystallographically independent molecules of **2** (with complete numbering scheme). An X-ray crystallographic file, in CIF format. See any current masthead page for Web access instructions.

---

(61) The reported PD_{film} value is the average value based on measurements with eight films in the $0.4-2.2$-μm thickness range.

(62) Pinhole defects are comparatively more important with thinner films: the thinnest low-defect-density films currently available using evaporative casting are 0.15 μm.

(63) The values of D_{sln} measured here were 8 $\times$ 10^{-6} ($Fe(CN)_6^{3-}$) and 5 $\times$ 10^{-6} cm^2 s^{-1} ($Ru(NH_3)_5py^{2+}$).

(64) The polycationic nature of the metallopolymers cited also introduces electrostatic effects that can significantly influence the values of permeant partition coefficients. (See: ref 31 and Ewing, A. G.; Feldman, B. J.; Murray, R. W. *J. Electroanal. Chem.* **1983**, *153*, 223.) A comparison of PD_{film} values obtained here to values obtained for similarly sized neutral permeants in charged framework metallopolymeric films, where electrostatic effects should be absent, still indicates a roughly 1 order of magnitude greater permeability for the metallocyclophane-derived materials.